Available online at www.sciencedirect.com
SCIENCE DIRECT®
Flow Measurement and Instrumentation 15 (2004) 285–293
Flow Measurement and Instrumentation
www.elsevier.com/locate/flowmeasinst

End depth computation in inverted semicircular channels using ANNs

R.V. Raikar [a,*], D. Nagesh Kumar [b], Subhasish Dey [a]

[a] Department of Civil Engineering, Indian Institute of Technology, Kharagpur West Bengal 721302, India
[b] Department of Civil Engineering, Indian Institute of Science, Bangalore 560012, Karnataka, India

Received 14 April 2003; accepted 11 June 2004

Abstract

The paper presents the application of artificial neural network (ANN) to determine the end-depth-ratio (EDR) for a smooth inverted semicircular channel in all flow regimes (subcritical and supercritical). The experimental data were used to train and validate the network. In subcritical flow, the end depth is related to the critical depth, and the value of EDR is found to be 0.705 for a critical depth–diameter ratio up to 0.40, which agrees closely with the value of 0.695 given by Dey [Flow Meas. Instrum. 12 (4) (2001) 253]. On the other hand, in supercritical flow, the empirical relationships for EDR and non-dimensional discharge with the non-dimensional streamwise slope of the channel are established.

Keywords: Artificial neural network; One-dimensional flow; Open channels; Steady flow

1. Introduction

A free overfall is a situation, causing the flow to separate from the streambed to form free nappe due to a sudden drop. It causes a gradually varying flow profile and also offers the possibility of being used as a flow-measuring device in all flow regimes (subcritical and supercritical). Earlier, in open channel hydraulics critical depth was used to determine the discharge, as there exists a unique relationship between critical depth and discharge. This method based on critical depth and discharge has a disadvantage, because the location of occurrence of critical depth is dependent on discharge that makes it difficult to measure. To overcome this problem of locating the position where the flow becomes critical, the attempts are made to relate the critical depth with end depth. The end depth is the flow depth at the free overfall, which also called as brink depth. Thus, the end depth is identified as key parameter for the flow measurement in open channel hydraulics. Fundamental experimental research was carried out by Rouse [2] to determine the end-depth-ratio (EDR), which was found to be 0.715 in mildly sloping rectangular channels. Since then numerous experiments on free overfall in different types of channels have been reported [1,3–42].

Rajaratnam and Muralidhar [3] explored circular overfalls by developing a theoretical model based on the momentum equation and experimental results. Numerical solutions using potential flow theory were presented by Montes [4]; whereas analytical solutions for circular overfalls based on the momentum equation and the simulation of a free overfall with a sharp-crested weir were given by Dey [5,6], respectively. The modified energy equation based on the Boussinesq approximation was used by Anderson [7] to determine the EDR for the rectangular overfall. Considering the streamline inclination and curvature, the solutions of momentum and extended energy equations were put forward by Hager [8]. Theory of direct fluid sheet was applied by Naghdi and Rubin [9] to develop an exact solution of the associated nonlinear equations. Another analytical approach, termed cnoidal wave theory, was reported by Marchi [10] to solve the two-dimensional

* Corresponding author. Tel.: +91-3222-283418; fax: +91-3222-282254.
E-mail address: raikar@civil.iitkgp.ernet.in (R.V. Raikar).

0955-5986/$ - see front matter © 2004 Elsevier Ltd. All rights reserved.
doi:10.1016/j.flowmeasinst.2004.06.003

Nomenclature

b	bias
D	channel diameter (m)
E	error
h	flow depth (m)
$\hat{h}$	h/D
$\tilde{h}$	h/h_c
P	number of training patterns
p	number of output nodes
Q	discharge ($m^3\ s^{-1}$)
$\hat{Q}$	$Q/(g^{0.5}\ D^{2.5})$
S	channel slope
$\hat{S}$	S/S_c
$\tilde{S}$	$(\hat{S}-1)/\hat{S}_{max}$
t	desired target
U	input vector $[u_1, u_2, \ldots, u_n]$
u	input value
W	weight vector $[w_{1j}, w_{2j}, \ldots, w_{nj}]$
w	weight of connection
x	distance along channel (m)
Y	output vector $[y_1, y_2, \ldots, y_n]$ and
y	network output

Subscripts

c	critical flow
e	end section
i	neuron of the previous layer
j	neuron of the successive layer and
o	far upstream section

free overfall. Also, the end depths in trapezoidal and exponential channels were analytically determined by Murty Bhallmudi [11] using the momentum approach based on the Boussinesq approximation. Anastasiadou-Partheniou and Hatzigiannakis [12] and Ferro [13] simulated the free overfall with a sharp-crested weir. The effect of bottom roughness on rectangular overfalls was studied by Dey [14,15]. Dey [1,16,18,19] and Dey and Ravi Kumar [17] studied free overfalls in circular channels with flat base, Δ-shaped, U-shaped and inverted semicircular channels, respectively. ISO 3874 [20] and ISO 4371 [21] recommended the estimation of discharge by the end depth method in rectangular and non-rectangular channels, respectively. Dey [22] put forward a comprehensive state-of-the-art review of researches on free overfall. However, little attempt has so far been made to analyze the free overfall by ANNs.

This paper presents an application of ANN to free overfall using experimental results for smooth inverted semicircular channels. The back-propagation algorithm based upon the generalized delta rule proposed by Rumelhart et al. [43] was used to train the ANN in this study. Part of experimental data is used to train the ANN and the remaining to validate. The ANN yields the EDR and discharge, which are compared with results of Dey [1].

2. Overview of ANNs

The development of ANNs began approximately 50 years ago [44], inspired by a desire to understand the human brain to emulate its functioning. Within the last decade, it has experienced a huge resurgence due to the development of more sophisticated algorithms and the emergence of powerful computational tools. Extensive research has been devoted in investigating the potential of ANNs as computational tools that acquire, represent and compute a mapping from one multivariate input space to another. Mathematically, an ANN is often used as a universal approximator. The ability of identifying a relationship from given patterns make it possible for ANNs to solve large-scale complex problems such as pattern recognition, nonlinear modeling, classification, association and control.

An ANN is a massively parallel-distributed information-processing system that has certain performance characteristics resembling biological neural networks of the human brain [45]. This development is based on the following rules:

1. Information processing occurs at many single elements called nodes, also referred to as units, cells or neurons.
2. Signals are passed between nodes through connection links.
3. Each connection link has an associated (synaptic) weight that represents its connection strength.
4. Each node typically applies a nonlinear transformation called an activation function to its net input to determine its output signal.

A neural network is characterized by its architecture that represents the pattern of connection between nodes, its method of determining the connection weights, and the activation function [46]. Usually, neural networks are classified based on the number of layers: single layer, multilayer; and based on the direction of information flow and processing: feed-forward, recurrent. A typical ANN consists of an input layer, an output layer and the hidden layers, each layer having a number of neurons (nodes). Fig. 1 shows the configuration of a feed-forward four-layer ANN. The input (first) layer of neurons receives the input variables for the problem at hand. This consists of all the quantities that can influence the output. The output (last) layer of neurons consists of values predicted by the network

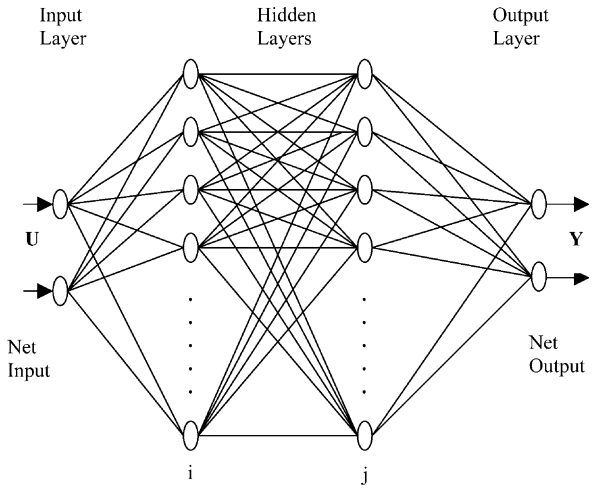

Fig. 1. Schematic representation of a feed-forward four-layer ANN.

and thus represents the model output. The number of hidden layers and the number of neurons in each hidden layer are usually determined by trial-and-error procedure. Each neuron in a layer is connected to all the neurons of the next layer by the connecting links, and the neurons in one layer are not connected among themselves. A synaptic weight is assigned to each link to represent the relative connection strength of two nodes at both ends in predicting input–output relationship. The data (signals) passing from a neuron of ith layer to the neuron of the jth layer (u_i) through the connecting link are multiplied by the respective synaptic weights. The output of the node j, y_j is obtained by computing the value of function f with respect to the inner product of vector U and W_j minus b_j, where b_j is the bias (or threshold value), associated with this node. The function f is called an activation function. Its functional form determines the response of a neuron to the total input signal it receives. Three basic types of activation functions are identified: threshold function, piecewise-linear function and sigmoid function. The most commonly used function is sigmoid function. This function is usually a steadily increasing S-shaped curve. Under this threshold function, the output y_j from the jth neuron in a layer is:

$$y_j = f(U.W_j - b_j) = \frac{1}{1 + e^{-(U.W_j - b_j)}} \quad (1)$$

where W_j = weight vector $[w_{1j}, w_{2j}, \ldots, w_{nj}]$; w_{ij} = weight of the connection joining the neuron of the jth layer with the neuron of the previous ith layer; U = input vector $[u_1, u_2, \ldots, u_n]$; and u_i = input value of the neuron in the ith layer.

In order for an ANN, to generate an output y_j that is as close as possible to the target t_j, a training process, also called learning, is employed to find optimal weight and bias, that minimizes a predetermined error function that usually has the form:

$$E = \sum_P \sum_p (y_j - t_j)^2 \quad (2)$$

where p is the number of output nodes; and P is the number of training patterns. Training is a process by which the connection weights of an ANN are adapted through a continuous process of simulation by the environment in which the network is embedded. There are primarily two types of training—supervised and unsupervised. A supervised training algorithm requires an external teacher to guide the training process. This implies that a large number of examples (or patterns) of inputs and outputs are required for training. The training procedure involves the iterative adjustment and optimization of connection weights and threshold values for each of nodes. On the other hand, an unsupervised training algorithm does not involve a teacher. During training, only an input data set is provided to the ANN that automatically adapts its connection weights to cluster those input patterns into classes with similar properties. The primary goal of training is to minimize the error function by searching for a set of connection strengths and threshold values that cause the ANN to produce outputs that are equal to or close to targets. After training has been accomplished, it is then hoped that the ANN is capable of generating reasonable results given new inputs. The commonly used training algorithms are back-propagation,

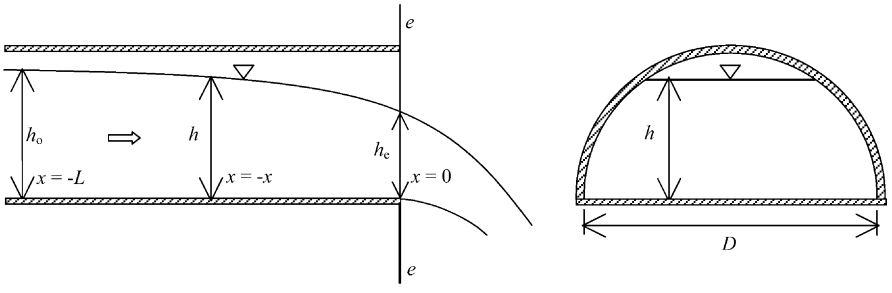

Fig. 2. Definition sketch of free overfall in an inverted semicircular channel.

Table 1
Experimental data in horizontal channels

Channel	D (mm)	Q ($m^3\ s^{-1}$)	$\hat{h}_c$	$\hat{h}_e$	$\tilde{h}_c$	$\hat{Q}$
1	128	4.604×10^{-4}	0.086	0.059	0.691	2.508×10^{-2}
		5.279×10^{-4}	0.094	0.066	0.706	2.875×10^{-2}
		6.442×10^{-4}	0.107	0.078	0.726	3.509×10^{-2}
		6.900×10^{-4}	0.112	0.082	0.728	3.758×10^{-2}
		2.083×10^{-3}	0.234	0.169	0.721	1.135×10^{-1}
		1.875×10^{-3}	0.218	0.149	0.684	1.021×10^{-1}
		1.701×10^{-3}	0.205	0.148	0.721	9.305×10^{-2}
		1.438×10^{-3}	0.183	0.124	0.677	7.830×10^{-2}
		8.429×10^{-4}	0.128	0.090	0.703	4.591×10^{-2}
		1.233×10^{-3}	0.165	0.118	0.717	6.718×10^{-2}
		1.029×10^{-3}	0.146	0.100	0.684	5.606×10^{-2}
		8.933×10^{-4}	0.133	0.098	0.734	4.866×10^{-2}
		7.771×10^{-4}	0.121	0.068	0.679	4.233×10^{-2}
		4.171×10^{-4}	0.080	0.055	0.680	2.272×10^{-2}
		2.179×10^{-3}	0.241	0.176	0.739	1.187×10^{-1}
		1.954×10^{-3}	0.224	0.161	0.719	1.064×10^{-1}
		5.829×10^{-4}	0.100	0.071	0.707	3.175×10^{-2}
		1.763×10^{-3}	0.209	0.143	0.681	9.600×10^{-2}
		1.550×10^{-3}	0.192	0.136	0.706	8.443×10^{-2}
		1.183×10^{-3}	0.161	0.109	0.680	6.445×10^{-2}
2	68	7.558×10^{-4}	0.337	0.231	0.685	1.998×10^{-1}
		5.158×10^{-4}	0.264	0.191	0.722	1.366×10^{-1}
		4.233×10^{-4}	0.232	0.163	0.704	1.121×10^{-1}
		2.804×10^{-4}	0.177	0.124	0.701	7.425×10^{-2}
		3.821×10^{-4}	0.217	0.158	0.727	1.012×10^{-1}
		2.521×10^{-4}	0.164	0.121	0.735	6.675×10^{-2}
		2.258×10^{-4}	0.153	0.104	0.678	5.980×10^{-2}
		5.988×10^{-4}	0.291	0.200	0.688	1.585×10^{-1}
		4.604×10^{-4}	0.245	0.178	0.728	1.219×10^{-1}
		4.250×10^{-4}	0.232	0.165	0.708	1.125×10^{-1}
		7.454×10^{-4}	0.334	0.236	0.706	1.974×10^{-1}
		6.475×10^{-4}	0.306	0.223	0.729	1.714×10^{-1}
		5.550×10^{-4}	0.277	0.187	0.674	1.470×10^{-1}
		4.954×10^{-4}	0.257	0.181	0.740	1.312×10^{-1}
		4.317×10^{-4}	0.235	0.166	0.706	1.143×10^{-1}
		7.875×10^{-4}	0.345	0.253	0.731	2.085×10^{-1}
		6.842×10^{-4}	0.317	0.223	0.704	1.812×10^{-1}
		6.713×10^{-4}	0.313	0.214	0.683	1.777×10^{-1}
		6.171×10^{-4}	0.296	0.214	0.720	1.634×10^{-1}
		5.800×10^{-4}	0.285	0.195	0.683	1.536×10^{-1}
3	43	2.495×10^{-4}	0.345	0.247	0.716	2.077×10^{-1}
		2.180×10^{-4}	0.317	0.224	0.708	1.815×10^{-1}
		1.811×10^{-4}	0.282	0.201	0.714	1.508×10^{-1}
		1.586×10^{-4}	0.258	0.180	0.696	1.320×10^{-1}
		1.358×10^{-4}	0.233	0.164	0.705	1.130×10^{-1}
		1.022×10^{-4}	0.191	0.137	0.716	8.344×10^{-2}
		7.095×10^{-5}	0.152	0.104	0.685	5.908×10^{-2}
		6.600×10^{-5}	0.145	0.102	0.703	5.496×10^{-2}
		5.520×10^{-5}	0.128	0.092	0.721	4.597×10^{-2}
		3.660×10^{-5}	0.098	0.067	0.689	3.047×10^{-2}
		2.646×10^{-4}	0.357	0.249	0.697	2.203×10^{-1}
		2.432×10^{-4}	0.339	0.237	0.697	2.025×10^{-1}
		2.829×10^{-4}	0.371	0.261	0.702	2.356×10^{-1}
		2.460×10^{-4}	0.342	0.243	0.710	2.048×10^{-1}
		1.977×10^{-4}	0.297	0.210	0.704	1.646×10^{-1}
		1.682×10^{-4}	0.268	0.186	0.694	1.400×10^{-1}
		1.511×10^{-4}	0.250	0.179	0.714	1.258×10^{-1}

Table 1 (*continued*)

Channel	D (mm)	Q ($m^3\ s^{-1}$)	$\hat{h}_c$	$\hat{h}_e$	$\tilde{h}_c$	$\hat{Q}$
		1.187×10^{-4}	0.213	0.150	0.703	9.880×10^{-2}
		7.815×10^{-5}	0.162	0.115	0.713	6.507×10^{-2}
		4.935×10^{-5}	0.119	0.081	0.681	4.109×10^{-2}

conjugate gradient algorithms, radial basis function and cascade correlation algorithm [47].

ANNs have been used in a wide range of areas in hydrology and hydraulics due to the successive applications in modeling nonlinear system behaviour. ANNs have been used for rainfall-runoff modeling, flow predictions, flow/pollution simulation, parameter identification, and modeling nonlinear/input–output time series [48,49].

3. Experimental set-up and procedure

The experiments were carried out in three different inverted semicircular channels (made of transparent perspex), having diameters 128 mm (Channel 1), 68 mm (Channel 2) and 43 mm (Channel 3). The lengths of the channels were 4 m. A flexible joint arrangement, acted as a hinge to provide the slope of any desired value. Fig. 2 shows the free overfall in a smooth inverted semicircular channel.

The discharge entering into the channel from a constant head tank fed by a centrifugal pump, was set by slowly opening the upstream valve until a desired height at the end section of the channel was reached. The corresponding discharge was recorded with the aid of a measuring tank. For each channel, two series of experiments were conducted for settings of horizontal and steep (supercritical) streamwise slopes. The end depths were measured by a point guage. Tables 1 and 2 present the experimental data for horizontal and steep slopes, respectively.

Table 2
Experimental data of steep sloping channels and comparisons with the computational data

Q ($m^3\ s^{-1}$)	$\hat{h}_c$	$\hat{h}_e$	S	$\tilde{S}$	$\tilde{S}'$	$\tilde{h}_e$	$\hat{Q}$
Channel 1 ($D = 128$ mm)							
7.857×10^{-4}	0.123	0.062	0.022	3.169	0.704	0.509	4.289×10^{-2}
8.663×10^{-4}	0.131	0.078	0.022	3.276	0.739	0.596	4.718×10^{-2}
4.967×10^{-4}	0.090	0.051	0.022	2.238	0.402	0.563	2.705×10^{-2}
6.858×10^{-4}	0.112	0.066	0.018	2.485	0.482	0.593	3.736×10^{-2}
4.875×10^{-4}	0.089	0.059	0.014	1.741	0.241	0.666	3.655×10^{-2}
7.492×10^{-4}	0.119	0.070	0.014	2.003	0.326	0.591	4.081×10^{-2}
8.146×10^{-4}	0.125	0.078	0.014	2.062	0.345	0.621	4.437×10^{-2}
8.575×10^{-4}	0.130	0.070	0.027	4.080	1.000	0.541	4.671×10^{-2}
Channel 2 ($D = 68$ mm)							
5.121×10^{-4}	0.263	0.139	0.019	3.634	0.855	0.532	1.356×10^{-1}
3.517×10^{-4}	0.205	0.114	0.019	3.074	0.673	0.554	9.312×10^{-2}
7.500×10^{-4}	0.335	0.200	0.015	3.532	0.822	0.597	1.986×10^{-1}
6.150×10^{-4}	0.296	0.159	0.015	3.180	0.708	0.537	1.628×10^{-1}
5.046×10^{-4}	0.260	0.163	0.015	2.887	0.603	0.627	1.336×10^{-1}
3.971×10^{-4}	0.222	0.131	0.015	2.590	0.516	0.589	1.051×10^{-1}
5.092×10^{-4}	0.262	0.173	0.013	2.479	0.480	0.660	1.348×10^{-1}
3.950×10^{-4}	0.222	0.145	0.013	2.210	0.393	0.654	1.046×10^{-1}
Channel 3 ($D = 43$ mm)							
2.552×10^{-4}	0.349	0.203	0.018	3.684	0.871	0.582	2.125×10^{-1}
1.854×10^{-4}	0.286	0.162	0.018	3.109	0.685	0.567	1.544×10^{-1}
1.755×10^{-4}	0.276	0.160	0.018	3.027	0.658	0.580	1.461×10^{-1}
1.575×10^{-4}	0.257	0.156	0.018	2.874	0.608	0.640	1.312×10^{-1}
2.007×10^{-4}	0.301	0.182	0.016	2.877	0.609	0.640	1.671×10^{-1}
1.800×10^{-4}	0.280	0.177	0.016	2.724	0.560	0.633	1.499×10^{-1}
1.575×10^{-4}	0.257	0.164	0.016	2.555	0.505	0.639	1.312×10^{-1}
1.305×10^{-4}	0.227	0.149	0.016	2.346	0.437	0.655	1.087×10^{-1}

Table 3
Parameters of network

Regime of flow	Input data		Number of neurons in the hidden layer	$\tilde{h}_e$			$\hat{Q}$		
	Training	Testing		Number of iterations	RMS error		Number of iterations	RMS error	
					Training	Testing		Training	Testing
Subcritical flow	50	50	3	68980	0.000115	0.001354	8900	0.000239	0.000456
	50	50	5	28650	0.000125	0.001269	45180	0.000247	0.000419
	50	50	7	9650	0.000138	0.001025	50585	0.000256	0.000405
	65	35	3	101425	0.000225	0.002514	125460	0.000118	0.000189
	65	35	5	96645	0.000211	0.002671	78565	0.000124	0.000164
	65	35	7	100875	0.000201	0.002698	8950	0.000138	0.000155
Supercritical flow	50	50	3	72290	0.000280	0.001070	7200	0.000242	0.000652
	50	50	5	11855	0.000250	0.001483	33135	0.000257	0.000553
	50	50	7	8305	0.000221	0.001755	5840	0.000256	0.000560
	65	35	3	1519470	0.000173	0.063079	22980	0.000168	0.000190
	65	35	5	105300	0.000320	0.001068	6945	0.000176	0.000204
	65	35	7	237680	0.000203	0.010195	5600	0.000158	0.000640

4. Results and discussion

A four-layer feed-forward ANN model is used to analyze the experimental data. The number of neurons in the hidden layers are varied from three to seven. The sigmoidal function is used as an activation function in the present study. The normalized data obtained from experimentation is divided into two parts, one part is used for training the network and the other for the validation of the performance of the network. Two combination of data grouping is considered for training and testing, 50:50 and 65:35. The values of learning rate parameter and momentum constant used are 0.2 and 0.5. The target error set for the network is 0.001 and the number of epochs 15. The other parameters like number of iterations, RMS error of training and testing for various network trials are given in Table 3.

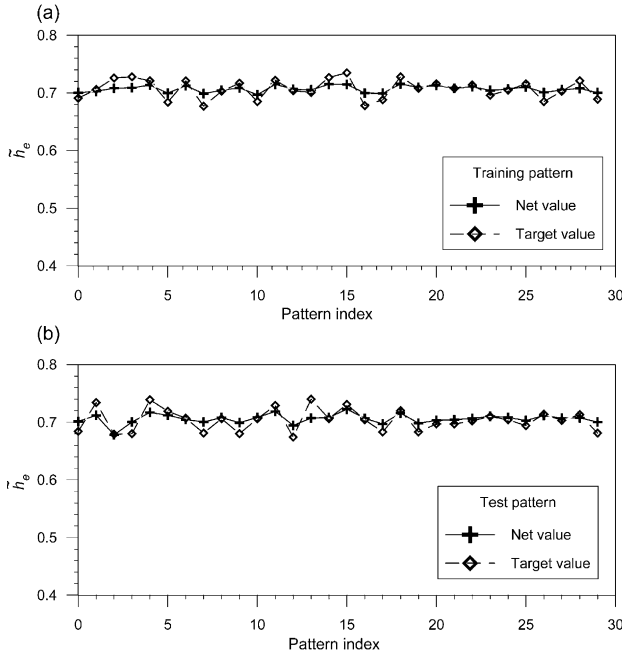

Fig. 3. Performance of ANN model in subcritical flow for $\tilde{h}_e$ (a) training; (b) testing.

4.1. Subcritical flow

The performance of the ANN model in the subcritical flow regime for EDR $\tilde{h}_e$ and non-dimensional discharge $\hat{Q}$ are shown in Figs. 3 and 4. The dependency of EDR $\tilde{h}_e$ on critical depth–diameter ratio $\hat{h}_c$ obtained from the network value is shown in Fig. 5. The value of EDR $\tilde{h}_e$ is found to be 0.705 up to $\hat{h}_c = 0.40$. The variation of $\hat{h}_e$ with $\hat{Q}$ is presented in Fig. 6. The variations, shown only in the range of the experimental data, correspond closely with Dey [1].

4.2. Supercritical flow

Figs. 7 and 8 show the performance of ANN model in supercritical flow regime for $\tilde{h}_e$ and $\hat{Q}$, respectively. The comparison of experimental data with net values for $\tilde{h}_e$ and $\hat{Q}$ is presented in Figs. 9 and 10 having regression coefficients 0.672 and 0.976, respectively. The empirical relationships are developed for EDR $\tilde{h}_e$ and non-dimensional discharge $\hat{Q}$ from the ANN output which can be used as ready reckoner to obtain the discharge from the measurement of end depth for a given slope.

$$\tilde{h}_e = 0.589\hat{h}_c^{0.0714}\tilde{S}^{-0.217} \quad (3)$$

$$\hat{Q} = 0.772\hat{h}_e^{0.874}\tilde{S}^{0.303} \quad (4)$$

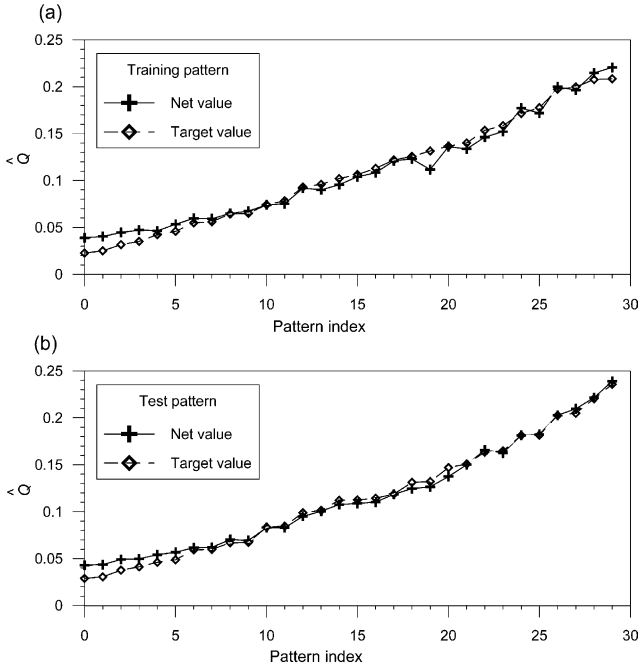

Fig. 4. Performance of ANN model in subcritical flow for $\hat{Q}$ (a) training; (b) testing.

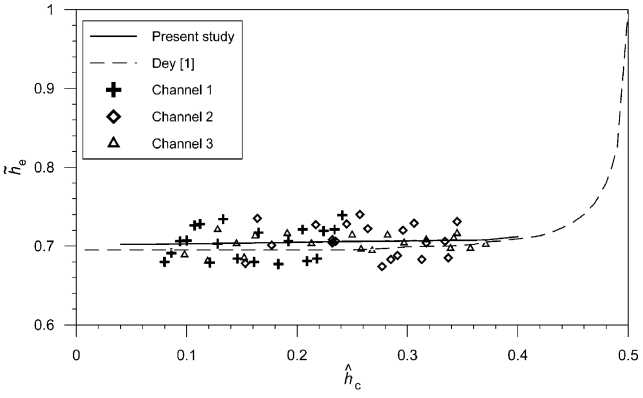

Fig. 5. Variation of EDR $\tilde{h}_e$ with $\hat{h}_c$ in subcritical flow.

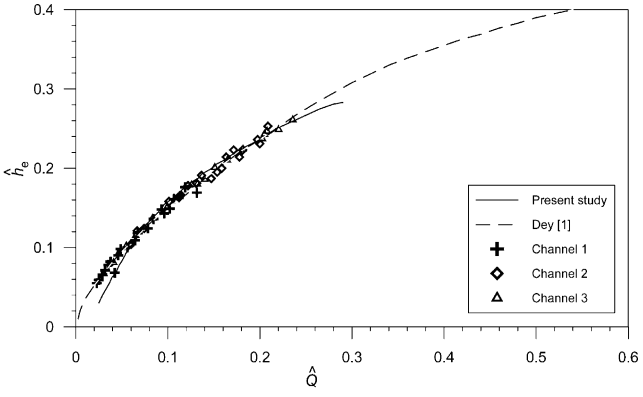

Fig. 6. Variation of EDR $\hat{h}_e$ with $\hat{Q}$ in subcritical flow.

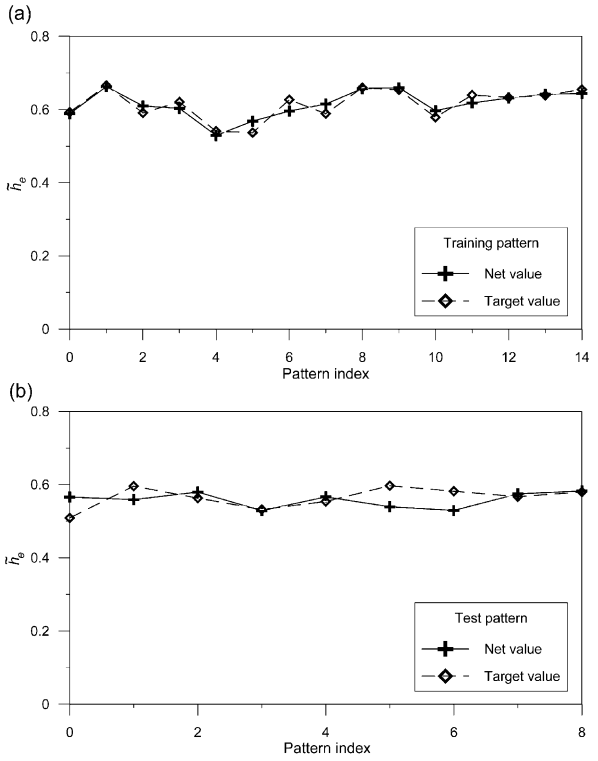

Fig. 7. Performance of ANN model in supercritical flow for $\tilde{h}_e$ (a) training; (b) testing.

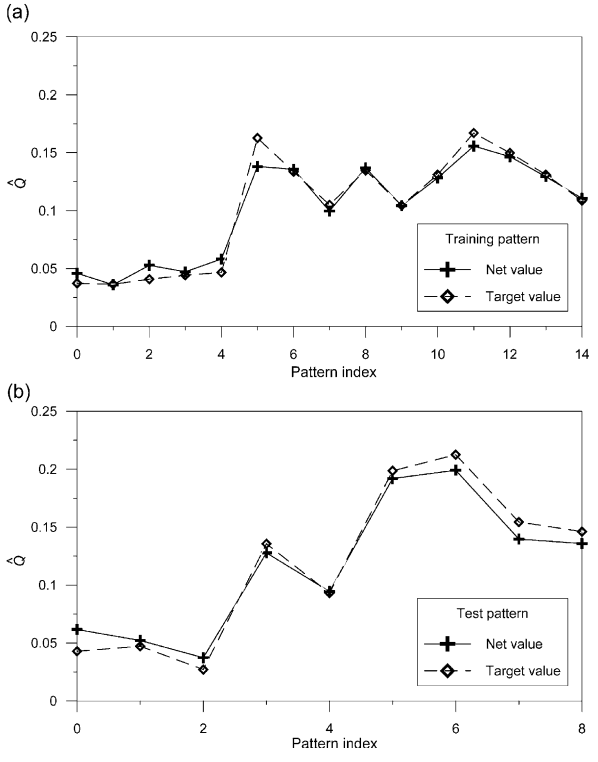

Fig. 8. Performance of ANN model in supercritical flow for $\hat{Q}$ (a) training; (b) testing.

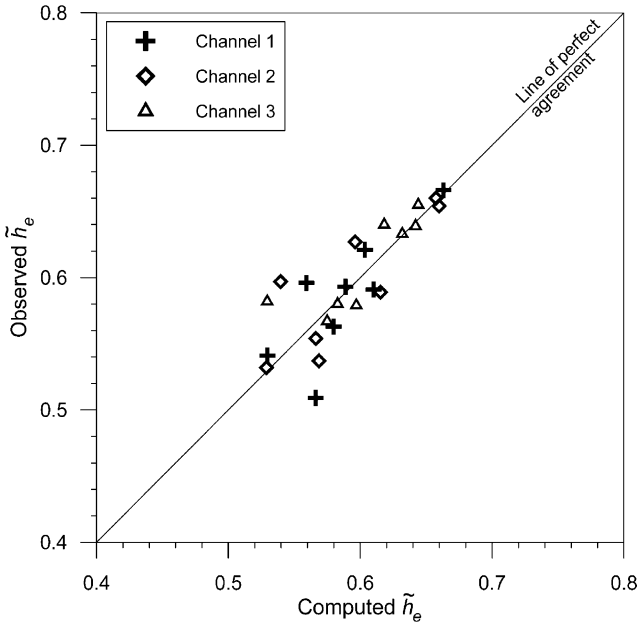

Fig. 9. Comparison of experimentally obtained $\tilde{h}_e$ with ANNs $\tilde{h}_e$ in supercritical flow.

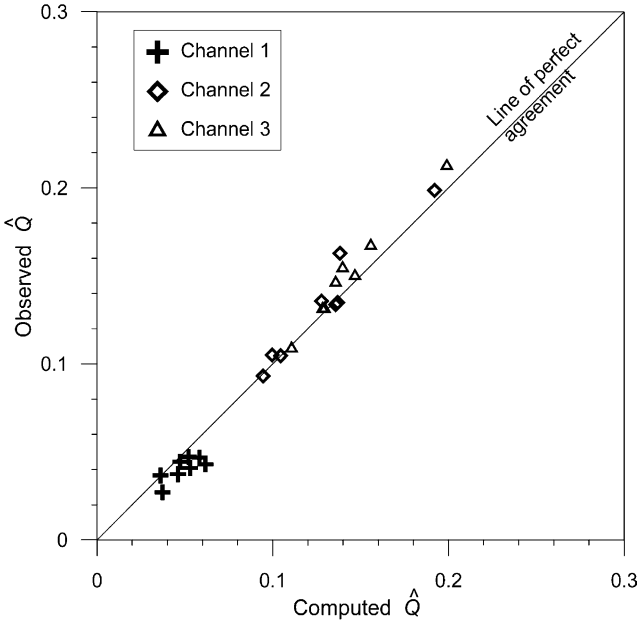

Fig. 10. Comparison of experimentally obtained $\hat{Q}$ with ANNs $\hat{Q}$ in supercritical flow.

5. Conclusions

A back-propagation algorithm based four-layer feed-forward ANN model has been used to determine the EDR and discharge for a smooth inverted semicircular channel in all flow regimes (subcritical and supercritical). The results of the network have corresponded closely with the results presented in Dey [1]. In subcritical flow, the EDR to the critical depth has been found to be 0.705 for $\hat{h}_c = 0.40$. For supercritical flow, the empirical relationships for EDR and non-dimensional discharge have been established.

References

[1] S. Dey, Flow measurement by the end-depth method in inverted semicircular channels, Flow Meas. Instrum. 12 (4) (2001) 253–258.
[2] H. Rouse, Discharge characteristics of the free overfall, Civ. Eng. ASCE 6 (4) (1936) 257–260.
[3] N. Rajaratnam, D. Muralidhar, End depth for circular channels, J. Irrig. Drain. Div. ASCE 90 (2) (1964) 99–119.
[4] J.S. Montes, A potential flow solution for the free overfall, Proc. Inst. Civ. Eng. (London), Water, Marit. Energy 96 (December) (1992) 259–266.
[5] S. Dey, End depth in circular channels, J. Hydraul. Eng. ASCE 124 (8) (1998) 856–863.
[6] S. Dey, The EDR in circular channels, J. Irrig. Drain. Eng. ASCE 127 (2) (2001) 110–112.
[7] M.V. Anderson, Non-uniform flow in front of a free overfall, Acta Polytech. Scand., Civ. Eng. Constr. Ser. 42 (1967) 1–24.
[8] W.H. Hager, Hydraulics of the plane overfall, J. Hydraul. Eng. ASCE 109 (2) (1983) 1683–1697.
[9] P.M. Naghdi, M.B. Rubin, On inviscid flow in a waterfall, J. Fluid Mech. 103 (1981) 375–387.
[10] E. Marchi, On the free overfall, J. Hydraul. Res. 31 (6) (1993) 777–790.
[11] S. Murty Bhallmudi, End depth in trapezoidal and exponential channels, J. Hydraul. Res. 32 (2) (1994) 219–232.
[12] L. Anastasiadou-Partheniou, E. Hatzigiannakis, General end-depth-discharge at free overfall in trapezoidal channel, J. Irrig. Drain. Eng. ASCE 121 (2) (1995) 143–151.
[13] V. Ferro, Theoretical end-depth-discharge relationships for free overfall, J. Irrig. Drain. Eng. ASCE 125 (1) (1999) 40–44.
[14] S. Dey, Free overfall in rough rectangular channels: a computational approach, Proc. Inst. Civ. Eng. (London), Water, Marit. Energy 130 (March) (1998) 51–54.
[15] S. Dey, End depth in steeply sloping rough rectangular channels, Sadhana, Proc. Indian Acad. Sci. 25 (February) (2000) 1–10.
[16] S. Dey, Free overfall from circular channels with flat base, Flow Meas. Instrum. 13 (5–6) (2002) 209–221.
[17] S. Dey, B. Ravi Kumar, Hydraulics of free overfall in Δ-shaped channels, Sadhana, Proc. Indian Acad. Sci. 27 (June) (2002) 353–363.
[18] S. Dey, Overfall in U-shaped channels, J. Eng. Mech. ASCE 129 (3) (2003) 358–362.
[19] S. Dey, Free overfall in inverted semicircular channel, J. Hydraul. Eng. ASCE 129 (6) (2003) 438–447.
[20] ISO 3874, End Depth Method for Estimation of Flow in Rectangular Channels with a Free Overfall, International Organization for Standardization, Geneva, Switzerland, 1977.
[21] ISO 4371, End Depth Method for Estimation of Flow in Non-Rectangular Channels with a Free Overfall, International Organization for Standardization, Geneva, Switzerland, 1984.
[22] S. Dey, Free overfall in open channels: state-of-the-art review, Flow Meas. Instrum. 13 (5–6) (2002) 247–264.
[23] N. Rajaratnam, D. Muralidhar, End depth for exponential channels, J. Irrig. Drain. Div. ASCE 90 (1) (1964) 17–36.
[24] R.J. Keller, S.S. Fong, Flow measurements with trapezoidal free overfall, J. Irrig. Drain. Eng. ASCE 115 (1) (1989) 125–136.
[25] V. Ferro, Flow measurement with rectangular free overfall, J. Irrig. Drain. Eng. ASCE 118 (6) (1992) 956–970.

[26] A.C. Davis, B.G.S. Ellett, R.P. Jacob, Flow measurement in sloping channels with rectangular free overfall, J. Hydraul. Eng. ASCE 124 (7) (1998) 760–763.
[27] K.H.M. Ali, A. Sykes, Free-vortex theory applied to free overfall, J. Hydraul. Div. ASCE 98 (5) (1972) 973–979.
[28] S.W. Bauer, W.H. Graf, Free overfall as measuring device, J. Irrig. Drain. Div. ASCE 97 (1) (1971) 73–83.
[29] W.L. Chow, T. Han, Inviscid solution for the problem of the free overfall, J. Appl. Mech. 46 (March) (1979) 1–5.
[30] N.S. Clarke, On two-dimensional inviscid flow in a waterfall, J. Fluid Mech. 22 (1965) 359–369.
[31] J.W. Delleure, J.C.I. Dooge, K.W. Gent, Influence of slope and roughness on the free overfall, J. Hydraul. Div. ASCE 82 (4) (1956) 30–35.
[32] M.H. Diskin, The end depth at a drop in trapezoidal channels, J. Hydraul. Div. ASCE 87 (4) (1961) 11–32.
[33] A. Fathy, M.A. Shaarawi, Hydraulics of free overfall, Proc. ASCE 80 Reston VA (1954) 1–12.
[34] R.D. Gupta, M. Jamil, M. Mohsin, Discharge prediction in smooth trapezoidal free overfall (positive, zero and negative slopes), J. Irrig. Drain. Eng. ASCE 119 (2) (1993) 215–224.
[35] C. Jaeger, Hauteur d'eau a l'extremite d'un long deversoir, La Houille Blanche 3 (6) (1948) 518–523.
[36] E. Markland, Calculation of flow at a free overfall by relaxation method, Proc. Inst. Civ. Eng. (London) 31 (May) (1965) 71–78.
[37] N. Rajaratnam, D. Muralidhar, Characteristics of rectangular free overfall, J. Hydraul. Res. 6 (3) (1968) 233–258.
[38] N. Rajaratnam, D. Muralidhar, The trapezoidal free overfall, J. Hydraul. Res. 8 (4) (1970) 419–447.
[39] N. Rajaratnam, D. Muralidhar, S. Beltos, Roughness effects on rectangular overfall, J. Hydraul. Div. ASCE 102 (5) (1976) 599–614.
[40] C.D. Smith, Brink depth for a circular channel, J. Hydraul. Div. ASCE 88 (6) (1962) 125–134.
[41] T. Strelkoff, M.S. Moayeri, Pattern of potential flow in a free overfall, J. Hydraul. Div. ASCE 96 (4) (1970) 879–901.
[42] S. Dey, Flow metering by end-depth method in elliptic channels, Dam Eng. 12 (1) (2001) 5–19.
[43] D.E. Rumelhart, J.L. McLelland PDP Research Group, Parallel distributed processing, explorations in the microstructure of cognition, Foundations, 1, MIT Press, Cambridge, MA, 1986.
[44] W.S. McCulloch, W. Pitts, A logical calculus of the ideas immanent in nervous activity, Bull. Math. Biophys. 5 (1943) 115–133.
[45] S. Haykins, Neural Networks: A Comprehensive Foundation, MacMillan, New York, 1994.
[46] L. Fausett, Fundamentals of Neural Networks, Prentice Hall, Englewood Cliffs, NJ, 1994.
[47] ASCE Task Committee on Application of Artificial Neural Networks in Hydrology, Artificial neural networks in hydrology. I: preliminary concepts, J. Hydraul. Eng. ASCE 5 (2) (2000) 115–123.
[48] ASCE Task Committee on Application of Artificial Neural Networks in Hydrology, Artificial neural networks in hydrology. II: hydrologic applications, J. Hydraul. Eng. ASCE 5 (2) (2000) 124–137.
[49] S.K. Jain, Development of integrated sediment rating curves using ANNs, J. Hydraul. Eng. ASCE 127 (1) (2001) 30–37.